J. Mol. Biol. (1998) **277**, 393–407

JMB

Crystal Structure of a Catalytic-site Mutant α-Amylase from *Bacillus subtilis* Complexed with Maltopentaose

Zui Fujimoto[1]*, Kenji Takase[1], Nobuko Doui[2], Mitsuru Momma[1] Takashi Matsumoto[1] and Hiroshi Mizuno[1,2]*

[1]*Department of Biotechnology National Institute of Agrobiological Resources Tsukuba, Ibaraki 305-8602, Japan*

[2]*Institute of Applied Biochemistry, University of Tsukuba, Tsukuba, Ibaraki 305-8572, Japan*

**Corresponding authors*

The X-ray crystal structure of a catalytic-site mutant EQ208 [Glu208 → Gln] of α-amylase from *Bacillus subtilis* cocrystallized with maltopentaose (G5) and acarbose has been determined by multiple isomorphous replacement at 2.5 Å resolution. Restrained crystallographic refinement has resulted in an *R*-factor of 19.8% in the 7.0 to 2.5 Å resolution range. EQ208 consists of three domains containing a $(\beta/\alpha)_8$-barrel as observed in other α-amylases. Clear connected density corresponding to a pentasaccharide was observed, which was considered as the G5 molecule based on the high affinity of EQ208 for G5 that could replace prebound acarbose or a possible transglycosylation product of acarbose. The conformation around the third α-(1,4)-glucosidic bond makes a sharp turn, allowing the substrate to fit into the L-shaped cleft. Aromatic residues build the walls of the substrate binding cleft and leucine residues form the inner curvature of the cleft. The amide nitrogen of Gln208 forms a hydrogen bond with the glucosidic oxygen in the scissile bond between Glc3 and Glc4 (Glc1 is the non-reducing end glucose residue of the substrate). This hydrogen-bonding manner may correspond to that of the protonated state of Glu208 in the initial kinetic complex between wild-type enzyme and substrate. The amide oxygen of Gln208 is anchored by two hydrogen bonds with Ala177 and a water molecule, assisting to make the amide proton point precisely to the place of the catalytic attack. The carboxyl oxygen atoms of the other catalytic-site residues Asp176 and Asp269 form hydrogen bonds with the oxygen atoms of Glc3. The carboxyl group of Asp176 has non-bonded contacts to the anomeric carbon atom and to the endocyclic oxygen atom of Glc3. These results suggest that Glu208 acts as a general acid and Asp176 as a general base. Glc3 forms seven hydrogen bonds with the surrounding protein groups and a stacking interaction with Tyr62, which is consistent with the fact that Glc3 has the lowest mean thermal factor of 13.2 $Å^2$ among the five sugar residues. Three calcium ions are found, one of which is positioned near the substrate binding site as found in other α-amylases and could contribute to stabilization of the structure of the active site.

Keywords: α-amylase; *Bacillus subtilis*; catalytic mechanism; X-ray crystal structure; mutant protein

Introduction

α-Amylase (α-1,4-glucan-4-glucanohydrolase, EC 3.2.1.1) catalyzes the hydrolysis of α-D-(1,4)-glucosidic linkages in starch, glycogen and various oligosaccharides, releasing α-anomeric products. This enzyme has been studied extensively from various aspects: structure and function, secretion, and industrial application. The three-dimensional X-ray structures have been reported for α-amylases

Abbreviations used: BLA, *Bacillus licheniformis* α-amylase; BSUA, *Bacillus subtilis* α-amylase; CGTase, α-cyclodextrin glucanotransferase; DN176, catalytic-site mutant [Asp176 → Asn] of BSUA; DN269, catalytic-site mutant [Asp269 → Asn] of BSUA; EQ208, catalytic-site mutant [Glu208 → Gln] of BSUA; G4, maltotetraose; G5, maltopentaose; G9, maltononaose; Glc, glucose unit; MIR, multiple isomorphous replacement; PPA, pig pancreatic α-amylase; r.m.s., root mean square; TAA, Taka-amylase A.

0022–2836/98/120393–15 $25.00/0/mb971599

from *Aspergillus oryzae* (Matsuura *et al.*, 1984; Swift *et al.*, 1991), *A. niger* (Boel *et al.*, 1990; Brady *et al.*, 1991), *Bacillus licheniformis* (Machius *et al.*, 1995), pig pancreas (Qian *et al.*, 1993; Larson *et al.*, 1994), human pancreas (Brayer *et al.*, 1995), human salivary gland (Ramasubbu *et al.*, 1996), and barley (Kadziola *et al.*, 1994). These studies have provided the overall fold of α-amylase. Despite differences in their amino acid sequences, they have similar three-dimensional structures with three domains: domain A consisting of a central $(\beta/\alpha)_8$-barrel flanking the active site, domain B overlaying the active site from one side and domain C consisting of a β-structure with a Greek-key motif.

Identification and roles of the catalytic residues of α-amylase have been under long debate. α-Amylases have conserved two aspartic acids and one glutamic acid, which are now considered the catalytic residues. Site-directed mutagenesis experiments on the presumed catalytic residues showed that the substitution of any of these residues caused almost complete loss of activity and suggested that all the three residues were important for activity (Holm *et al.*, 1990; Vihinen *et al.*, 1990; Takase, 1992; Takase *et al.*, 1992; Søgaard *et al.*, 1993). Further understanding of the catalytic mechanism has been gained through the X-ray structure analysis of α-amylase complexed with substrate analogs. Pig pancreatic α-amylase (PPA) with an acarbose derivative (Qian *et al.*, 1994) and PPA isozyme II with the pseudo-octasaccharide inhibitor (Machius *et al.*, 1996) revealed that Glu233 is the most appropriate candidate for the general acid in the first stage of the catalytic process. Similar studies of the complex have progressed also in Taka-amylase A (TAA; α-amylase from *A. oryzae*; Brzozowski & Davies, 1997) and in α-cyclodextrin glucanotransferases (CGTases), which have domains A, B and C similar to α-amylases, and additional domains D and E (Strokopytov *et al.*, 1995, 1996).

On the other hand, structural studies using natural substrates have been reported. In CGTase crystals soaked with α-cyclodextrin or maltoheptaose, a maltotetraose (G4) molecule was observed to be bound in the active site (Knegtel *et al.*, 1995); use of a double mutant of catalytic residues also led to the structure with bound G4 possibly due to the residual activity of the mutant. Similarly, Klein *et al.* (1992) reported that crystals of a catalytic-site mutant CGTase soaked with β-cyclodextrin gave density corresponding to a maltose bound at the catalytic center. In the case of α-amylase, soaking of crystals of TAA with maltotriose resulted in the presence of only a single maltose residue in the active site (Matsuura *et al.*, 1984); PPA crystals soaked with maltopentaose (G5) revealed only maltose and glucose bound at sites distinct from the active site (Qian *et al.*, 1995). Recently, a G4 molecule was found in the analysis of a catalytic-site mutant of G4-forming exo-amylase cocrystallized with G5 (Yoshioka *et al.*, 1997). These results indicate that substrates were degraded by the enzymes during the soaking process or the crystallization. Therefore, a completely inactive enzyme is indispensable for the formation of a stable complex with natural substrate.

In our previous studies, we created three catalytic-site mutants of *B. subtilis* α-amylase (BSUA) by site-directed mutagenesis: DN176 [Asp176 → Asn], EQ208 [Glu208 → Gln], and DN269 [Asp269 → Asn]. These mutants are thought to be completely devoid of catalytic activity but retain substrate binding activity (Takase, 1992; Takase *et al.*, 1992). In the present study we have successfully obtained crystals of a complex of EQ208 with G5 suitable for X-ray diffraction analysis. The crystal structure of the complex has been determined at 2.5 Å resolution and revealed a well-defined density corresponding to five sugar residues. The obtained model demonstrates that the amide proton of the side-chain of Gln208 points to the site of catalytic attack. We describe here details of the substrate-binding interactions and discuss a possible catalytic mechanism.

Results

Quality of the final model

For the reasons described in the Discussion, we assume that the bound sugar is G5. The final model of BSUA-EQ208/G5 complex is made up of 425 amino acid residues and one G5 molecule. Of the total 438 amino acid residues deduced from the DNA sequence, N-terminal residues −2 and −1 and C-terminal residues 426 to 436 are excluded from the model. The crystallographic *R*-factor is 19.8% and the free *R*-factor is 25.2% for the data from 7 to 2.5 Å resolution (Brünger *et al.*, 1987; Brünger, 1992). Crystal parameters and refinement statistics are listed in Table 1. The mean positional error of the atoms as estimated from a Luzzati plot (Luzzati, 1952) is 0.27 Å. In a Ramachandran plot (Ramachandran & Sasisekharan, 1968), more than 85% of the non-glycine residues were in the most favored regions of a phi–psi plot while the remainder were in additional allowed regions. The bound G5 molecule was clearly observed in the MIR, $F_{obs} - F_{calc}$ and $2F_{obs} - F_{calc}$ electron density maps. Figure 1 shows that the agreement between the current model of G5 and the $F_{obs} - F_{calc}$ omit map with the calculated structure factors obtained by omitting G5 is quite satisfactory. The $2F_{obs} - F_{calc}$ maps contoured at 1σ show continuous density for all main-chain atoms except the terminal residues 1 to 3 and 425. These residues might be disordered.

The overall structure of BSUA

BSUA consists of a single polypeptide chain with approximately 26% α-helix and 22% β-sheet and has dimensions of approximately 35 Å × 40 Å × 70 Å. It has three domains as observed in other α-amylases (Figure 2). The cen-

Table 1. Crystal parameters and refinement statistics

Cell parameters ($P2_12_12_1$)	
a (Å)	72.6
b (Å)	74.1
c (Å)	117.0
Solvent content (%)	58
Refinement range (Å)	7–2.5
No. of reflections in refinement	17,162
R-factor (%)	19.8
R_{free} factor (%)	25.2
No. of all non-hydrogen atoms	3490
No. of protein non-hydrogen atoms	3285
No. of G5 non-hydrogen atoms	56
No. of calcium ions	3
No. of water molecules	146
Average *B*-factor (Å^2)	15.9
Protein atoms (Å^2)	15.5
G5 atoms (Å^2)	19.0
Calcium ions (Å^2)	11.6
Water molecules (Å^2)	24.0
r.m.s. deviations	
Bond lengths (Å)	0.007
Bond angles (deg)	1.4
Dihedral angles (deg)	24.3

R-factor is defined as $R = \Sigma | |F_o| - |F_c| | / \Sigma |F_o|$. R_{free} factor was calculated using 10% of the unique reflections.

tral part (domain A, Leu1 to Ile100 and Thr152 to Gly347) comprises $(\beta/\alpha)_8$-barrel, which is a commonly occurring motif first observed in triose phosphate isomerase (Banner *et al.*, 1975). The long active site cleft is located on the C-terminal side of the central β-barrel of domain A and is overlaid by the prominent excursion part (domain B, Asn101 to Asn151) from one side. The C-terminal region (domain C, Gln348 to Asp425) comprises eight β-strands containing a Greek key motif.

A topological alignment of BSUA, PPA, TAA, *B. licheniformis* α-amylase (BLA) and CGTase has been performed (Figure 3). Almost all β-strands and α-helices of the $(\beta/\alpha)_8$-barrel in domain A and Greek key motif in domain C are conserved for all proteins. Domain B is the most variable region, as only β-strands at both ends and one α-helix are conserved. BSUA has the shortest length of domain B among them, while another bacterial α-amylase BLA has a unique structure of domain B in that it is exceptionally long and does not possess the conserved α-helix Bα1 (Machius *et al.*, 1995).

The stereoview of the superpositioned C^α models of BSUA and PPA is shown in Figure 4. Although the entire peptide length of BSUA is shorter than PPA due to deletions in some loop regions (the middle part of domain B, between Aβ8 and Aα8 and between Cβ5 and Cβ6; Figure 3), the overall structures of the two α-amylases, especially the core region of the $(\beta/\alpha)_8$-barrel, are in good agreement.

The active site and substrate binding

The final model of the enzyme/substrate complex allows for a detailed analysis of the interactions between G5 and EQ208. Figure 5 shows the G5-binding structure of EQ208, and Figure 6 shows a schematic drawing of the hydrogen-bonding network between EQ208 and G5. The five glucose units of G5 are numbered 1 to 5 from the

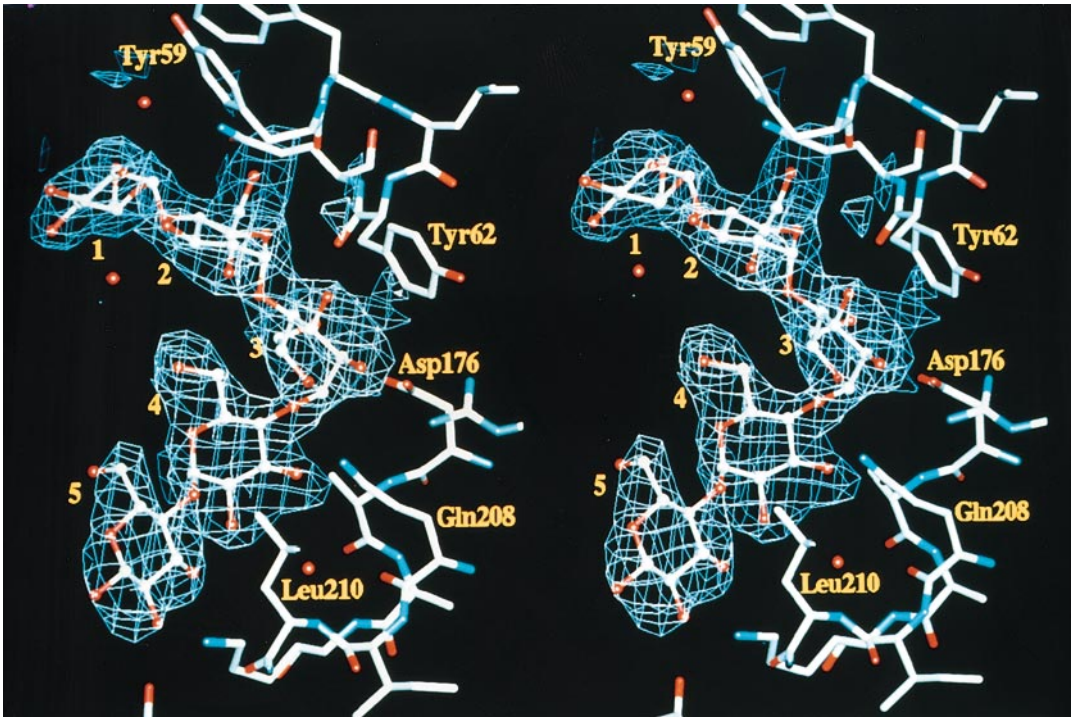

Figure 1. Stereoview of a $F_{obs} - F_{calc}$ omit electron density map for the carbohydrate ligand together with the refined model at 2.5 Å resolution. The map is contoured at 1.8 σ. The glucose residues are numbered from the non-reducing end.

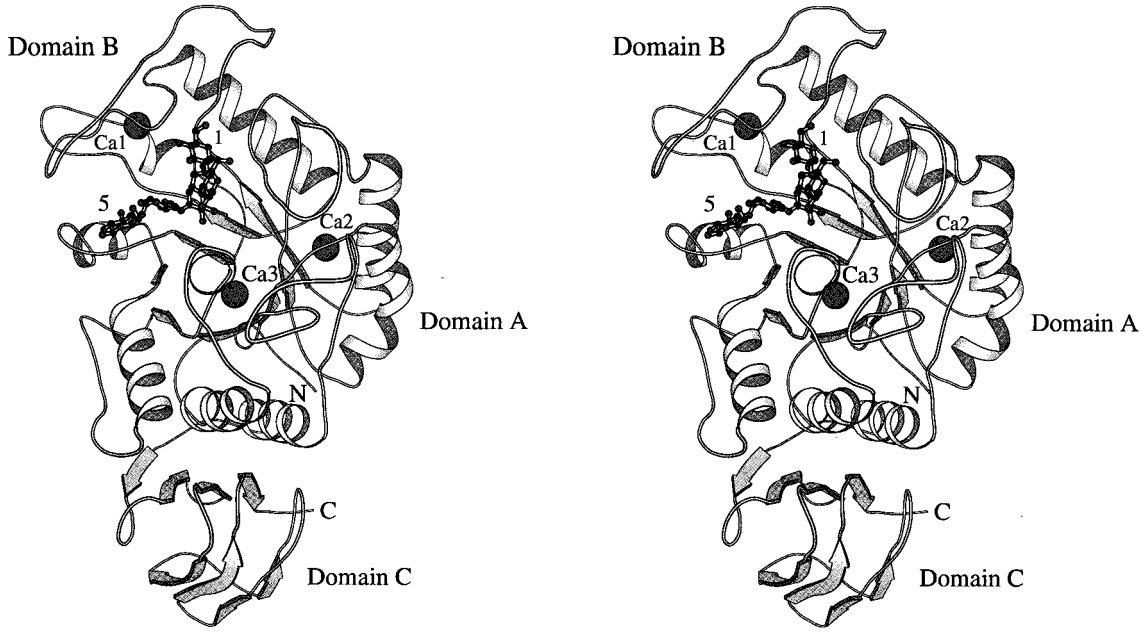

Figure 2. Stereoview of the ribbon model of the EQ208/G5 complex generated with the program MOLSCRIPT (Kraulis, 1991). The G5 molecule is indicated as a ball-and-stick plot and both end residues are numbered. Three calcium ions are shown as spheres.

non-reducing end toward the reducing end (Glc1-5). Table 2 shows the hydrogen bonding interactions in comparison with those of the PPA/acarbose derivative, TAA/acarbose derivative, CGTase/G9 inhibitor and CGTase/acarbose. Table 3 shows the hydrophobic interactions in comparison with those of the PPA/acarbose and CGTase/acarbose.

Glc1 is positioned in a hydrophobic pocket formed by the three aromatic rings of Tyr59, Trp60 and Phe105 and two side-chains of Leu142 and Leu144. A water molecule is positioned in a pocket formed by the main-chain atoms of Gln63, Phe105 and Leu144 and mediates hydrogen bonds between NE2 of Gln63 and the oxygen atoms O5 of Glc1 (hereafter O5(1)) and O6(1). O2(1) is involved in an internal hydrogen bond with the O3(2) of the adjacent glucose. Glc1 has no direct hydrogen bonds with the protein atoms in the complex, while an intermolecular hydrogen bond is observed between O2(1) and the side-chain of Lys27 of the symmetry-related protein molecule. Glc2 participates in three hydrogen bonds with three protein residues: Tyr59 and Gln63 are at the bottom of the cleft and Asn273 is near the molecular surface. Aromatic rings of Trp58 and Tyr59 make a hydrophobic wall on one side of Glc2 and Leu142 on the other side.

Glc3 is buried deeply at the bottom of the cleft, and tightly bound by seven hydrogen bonds and a stacking interaction with Tyr62. The hydrogen bonding residues His102, Arg174 and Asp176 are at the bottom of the cleft and Asp269 is near the molecular surface. The O2(3) and O3(3) hydroxyl groups do not participate in the internal O2–O3′ hydrogen bonds, instead they contribute to two bifurcated hydrogen bonds between OD1 of Asp269 and NE2 of His268 and between OD2 of Asp269 and NE2 of His268.

The catalytic reaction is considered to occur at the α-(1,4)-glucosidic bond between Glc3 and Glc4, releasing Glc4 and Glc5 as a maltose molecule (Robyt & French, 1970). Kinetic studies of a related *B. subtilis* α-amylase revealed five subsites with the cleavage point between subsite 3 and 4 (Hiromi *et al.*, 1983). The three catalytic-site residues Asp176, Gln208 and Asp269 form a triangle around it. The mutated residue Gln208 forms two hydrogen bonds with oxygen atoms of Glc4; one with the O4(4) oxygen atom of the third α-(1,4)-glucosidic bond through its amide amino group and one with the O3(4) hydroxyl group through its amide carbonyl. A water molecule buried in the vicinity has a considerably low thermal factor of 3.2 Å, and mediates interactions between Glc4 and the protein by five hydrogen bonds. This water molecule is likely to exist as a bound water for assisting stabilization of a local conformation of the protein and for binding the substrate. A similar water molecule is observed in PPA complexed with acarbose (Qian *et al.*, 1994) and CGTases complexed with acarbose, G9 inhibitor and G4 (Knegtel *et al.*, 1995; Strokopytov *et al.*, 1995, 1996). The O2(4) hydroxyl group forms a hydrogen bond with the side-chain of His180, which is also involved in calcium binding through its carbonyl oxygen. Glc4 has hydrophobic interactions with Leu141 on one side and with Leu210 on the other side. There exists an internal hydrogen bond between O2(4) and O3(5). Glc5 makes three hydrogen bonds with side-chains of Lys179 and Asp212,

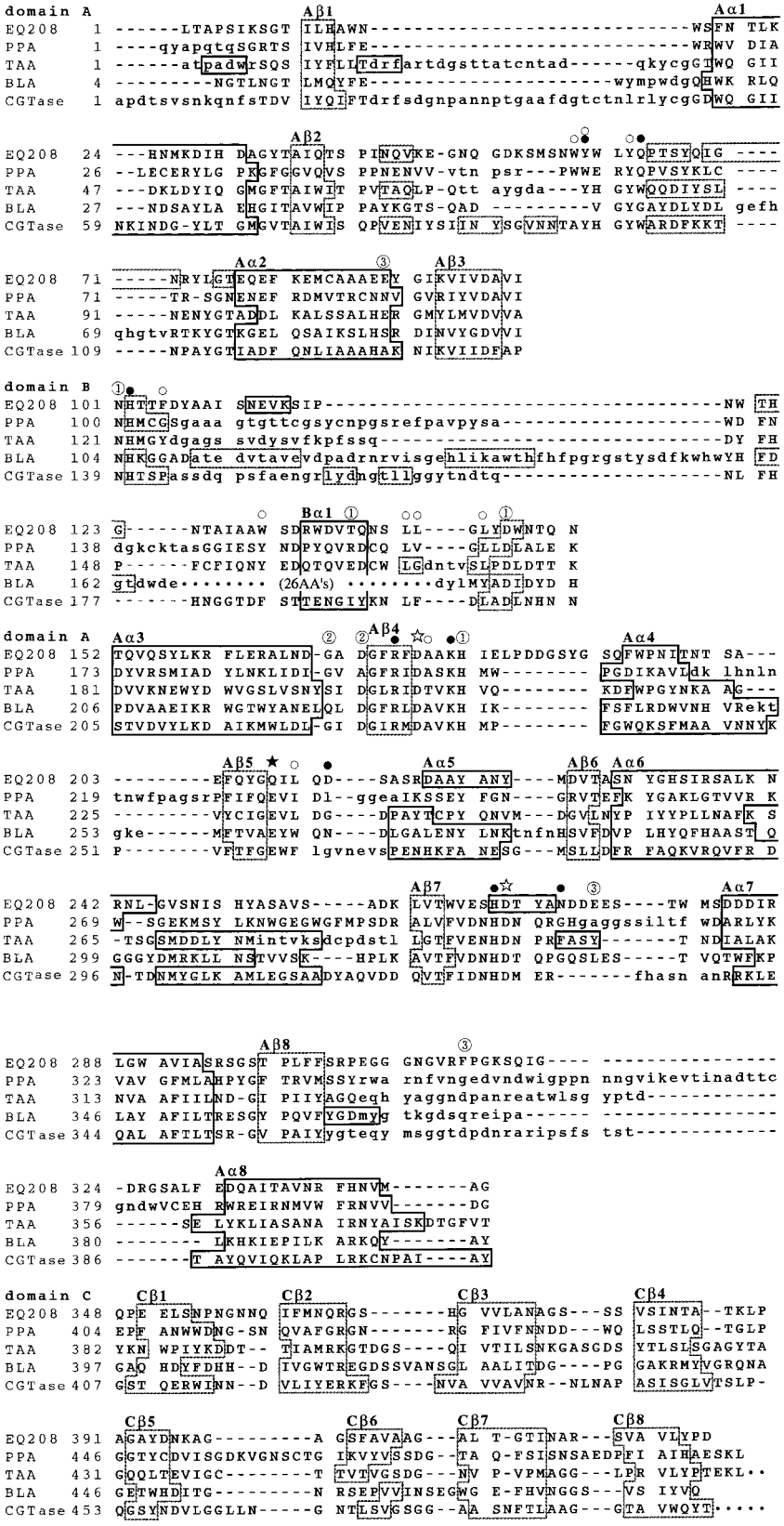

Figure 3. Topological alignment of BSUA (EQ208) with PPA (Qian *et al.*, 1994), TAA (Swift *et al.*, 1991), BLA (Machius *et al.*, 1995) and CGTase from *B. circulans* (Strokopytov *et al.*, 1996). Alignment was prepared based on the superpositioned models. Small letters indicate unpaired residues in this alignment. Residues that belong to α-helices and β-strands are surrounded by ▭ and ▭, respectively. Residues involved in each calcium binding are indicated with ①, ② and ③. The catalytic-site residues are indicated with ☆ or ★, where ★ represents the mutated residue. Residues involved in the hydrophilic and hydrophobic interactions with G5 are indicated with ● and ○, respectively. 26 amino acid residues of a central part of domain B of BLA, C-terminal residues of TAA and domain D and domain E of CGTase are omitted. Conserved secondary structures are named.

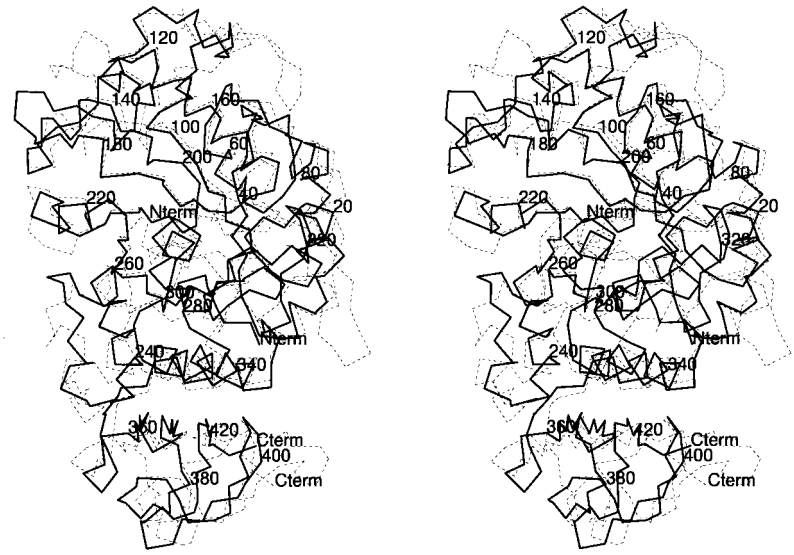

Figure 4. Stereoview of the superpositioned C^{α} models of EQ208 (——) and PPA (-----). EQ208 is numbered every 20 residues.

and a stacking interaction with Trp130 on one side. The other side of Glc5 is exposed to solvent.

The average thermal factors of G5 residues 1 to 5 are 20.9, 16.2, 13.2, 15.3 and 28.9 Å^2, respectively. Glc3 is thus tightly bound in the active site. This is apparently due to seven hydrogen bonds with six surrounding residues and stacking interaction with Tyr62. The average thermal factor of the surrounding residues interacting with Glc3 is 8.9 Å^2. These low averaged thermal factors and the $2F_{obs} - F_{calc}$ and the $F_{obs} - F_{calc}$ electron density maps around G5 indicate that the absolute occupancy of G5 is close to unity. The exceptionally high thermal fac-

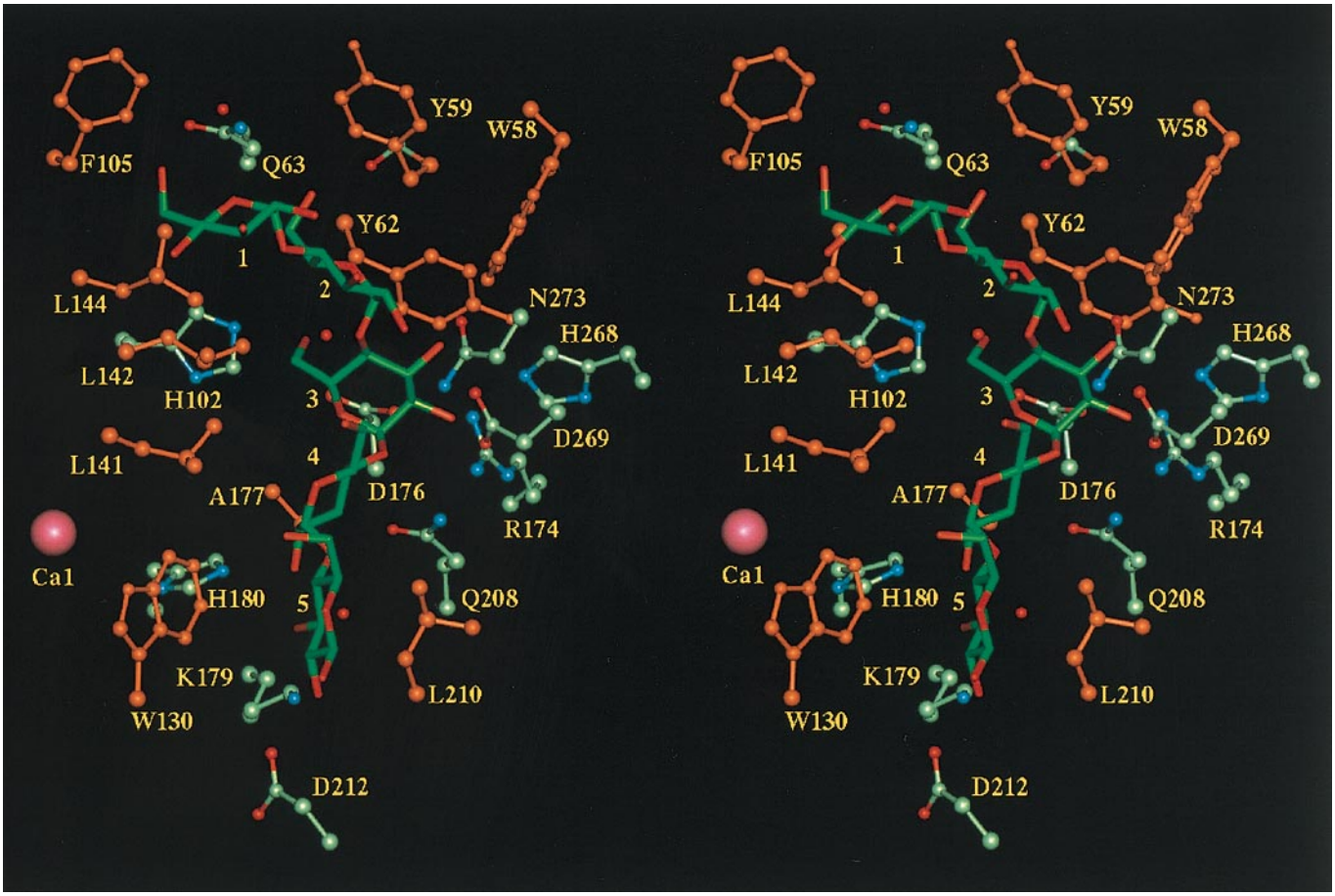

Figure 5. Stereoview of the G5-binding structure of EQ208. Residues involved in the hydrophilic interaction are colored by elements and those in the hydrophobic interaction are shown in orange.

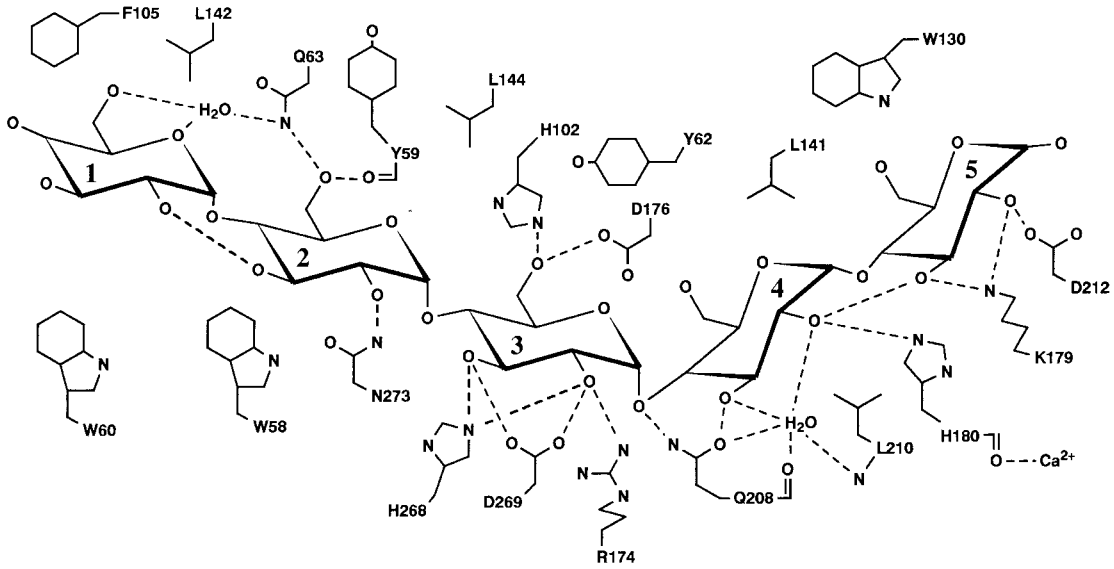

Figure 6. Schematic drawing of the hydrogen-bonding network between EQ208 and G5. Two water molecules mediating hydrogen bonds and hydrophobic residues interacting with G5 are also indicated.

tor of Glc5 may come from the fact that one side of Glc5 is exposed to solvent. In contrast, in the case of PPA, the glycine-rich loop after Aβ3 overlays the end of substrate binding site (Qian *et al*., 1994) and could reduce the motion of Glc5.

G5 conformation

Figure 7 illustrates a surface potential model of EQ208 with bound G5. The L-shaped binding cleft is clearly seen and there are hydrophobic walls on

Table 2. Hydrogen bonding interactions in the enzyme/substrate (inhibitor) complex. Sugar atom names are for the G5 molecule

		BSUA-EQ208/G5		PPA/acarbose derivative[b]	TAA/acarbose derivative[c]	CGTase/G9 inhibitor[d]	CGTase/ acarbose[e]
Sugar no.	Sugar atom	Protein atom	Distance (Å)	Protein atom	Protein atom	Protein atom	Protein atom
1	O2	(Lys27 NZ)[a]	2.6				
1	O3				Gln35 NE2		
1	O4			Val163 O			
1	O5			Gln63 NE2			
1	O6			Val163 O		Asp196 OD2	
2	O2	Asn273 ND2	2.8	His305 ND1	Arg344 NH1	Arg375 NH1	Arg375 NH1
2	O3					Arg375 NH2	Arg375 NH2
2	O3				Asp340 OD2	Asp371 OD2	Asp371 OD2
2	O6	Tyr59 O	2.6	Trp59 O			
2	O6	Gln63 NE2	3.2	Gln63 NE2	Trp83 NE1		
3	O2	Asp269 OD2	2.7	Asp300 OD1	Asp297 OD2	Asp328 OD2	Asp328 OD2
3	O2	His268 NE2	2.8	His299 NE2			His327 NE2
3	O2	Arg174 NH1	3.2		Arg204 NH1		
3	O3	His268 NE2	3.2	His299 NE2		His327 NE2	His327 NE2
3	O3	Asp269 OD1	3.2		Asp297 OD2		Asp328 OD1
3	O6	Asp176 OD1	3.2	Asp197 OD1	Asp206 OD2		Asp229 OD1
3	O6	His102 NE2	2.9	His101 NE2	His122 NE2		
4	O2	His180 NE2	2.7	His201 NE2	His210 NE2	His233 NE2	His233 NE2
4	O3	Gln208 OE1	2.7	Glu233 OE2	Glu230 OE2	Glu257 OE2	Glu257 OE2
4	O4	Gln208 NE2	2.9	Glu233 OE1	Glu230 OE1	Glu257 OE1	Glu257 OE1
4	O4						Glu 257 OE2
5	O2	Lys179 NZ	3.0	Lys200 NZ	Lys209 NZ		Lys232 NZ
5	O3	Asp212 OD2	2.8				
5	O3	Lys179 NZ	2.6	Lys200 NZ	Lys209 NZ	Lys232 NZ	Lys232 NZ

[a] Symmetry-related intermolecular contact.
[b] Qian *et al*. (1994).
[c] Brzozowski & Davies (1997).
[d] Strokopytov *et al*. (1996).
[e] Strokopytov *et al*. (1995).

Table 3. Hydrophobic interactions in the enzyme/substrate (inhibitor) complex

BSUA-EQ208/G5 Protein residue	Sugar no.	PPA/acarbose derivative[a] Protein residue	CGTase/acarbose[b] Protein residue
Phe105	1		
Tyr59	1, 2	Trp59	
Leu142	1, 2, 4	Val163	Phe195
Trp58	2, 3	Trp58	
Tyr62	2, 3	Tyr62	Tyr100
Leu141	3	Leu162	Leu194
Leu144	3	Leu165	Leu197
Ala177	4	Ala198	Ala230
Leu210	4	Ile235	Phe259
Trp130	5	Tyr151	Phe183

Sugar numbers are for the G5 molecule. Corresponding residues in PPA/acarbose derivative complex and CGTase/acarbose complex are listed.

[a] Qian *et al*. (1994).

[b] Strokopytov *et al*. (1995).

both sides of the cleft. The catalytic center lies at the bottom center of the cleft. The G5 molecule makes a sharp turn around Glc3. Table 4 shows the conformation of the bound G5 in terms of the torsion angles around its α-(1,4)-glucosidic bonds and the lengths between oxygen atoms of the O2 and the O3 hydroxyl groups of the adjacent glucoses. In general, malto-oligosaccharides are considered to take a gentle helical conformation with O2-O3′ hydrogen bonds and the torsion angles close to those observed in the crystal structure of α-maltose: 116° around O5-C1-O4′-C4′ and −118° around the C1-O4′-C4′-C5′ (Takusagawa & Jacobson, 1978). The conformation around the first and the fourth glucosidic bond of the bound G5 takes a helical structure. Torsion angles around the second glucosidic bond are somewhat different from those in the helical conformation, and coupled with O2–O3′ length, which is just longer than a hydrogen bond. This observation is similar to the structure of PPA/acarbose derivative complex (Qian *et al*., 1994; Machius *et al*., 1996). The conformation around the third glucosidic bond represents a kink conformation which enables G5

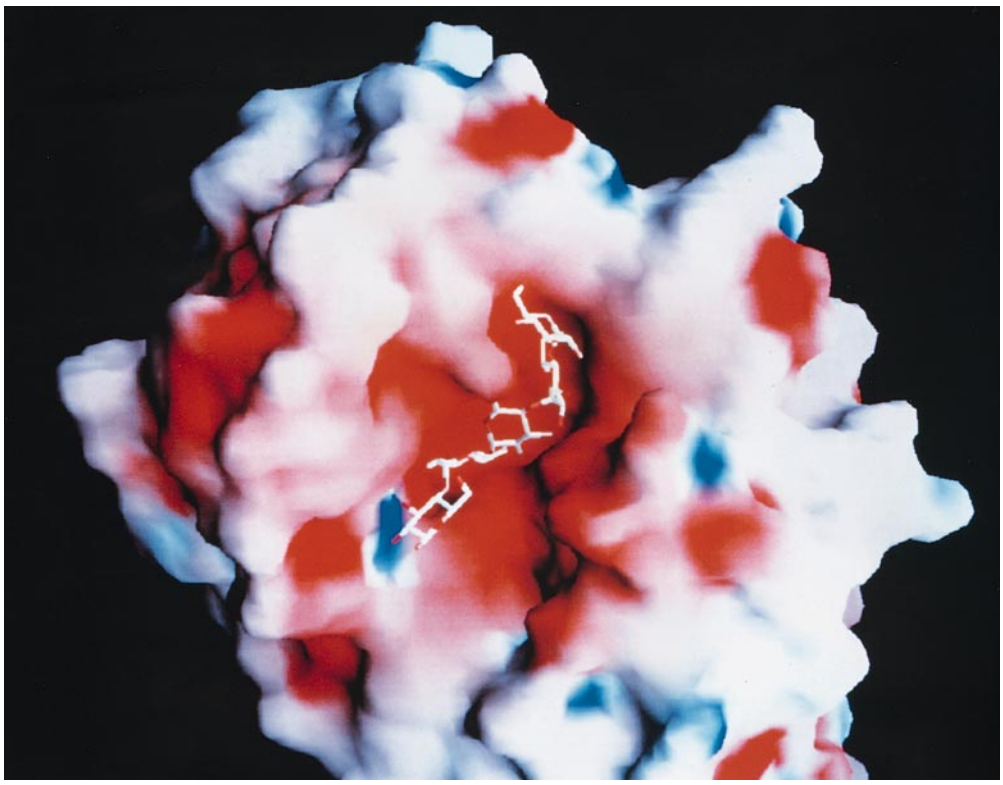

Figure 7. Surface potential model generated with the program GRASP (Nicholls, 1992). The potential represents a range from −10 to 10 kT, shown in red for negative and blue for positive. G5 molecule is bound in the active site cleft.

Table 4. Torsion angles around the glucosidic bonds and inter-sugar distances (O2–O3′) of G5 bound in the active site

Sugar residues	O5-C1-O4′-C4′ (°)	C1-O4′-C4′-C5′ (°)	O2–O3′ (Å)
1–2	127.2	−107.2	2.7
2–3	86.0	−153.7	3.6
3–4	25.5	−148.6	5.0
4–5	109.7	−116.8	2.7

to fit into the L-shaped cleft and to guide Glc3 into the catalytic center. However, this conformation is energetically not unfavorable and indeed near the second low-energy region of maltose (Dowd *et al.*, 1992).

The calcium binding site

Calcium binding site is generally observed in mammalian, barley and fungal α-amylases. In bacterial α-amylases, only the crystal structure of BLA is reported in its calcium-depleted form (Machius *et al.*, 1995; Hwang *et al.*, 1997). In the BSUA structure, three calcium ions were assigned on the basis of the electron density, the coordinating distances between calcium and protein atoms and appropriate coordination spheres. The coordinating residues of the three calcium binding sites are marked in Figure 3 and coordinating protein atoms and their distances to the calcium ions are listed in Table 5.

The conserved calcium binding site superpositioned with that of the other α-amylases is shown in Figure 8. It is apparent that the structure of this Ca-1 binding site is strictly conserved among α-amylases except BLA, where the calcium ion is not present. In BLA, there is a water molecule instead and no residue corresponding to Thr137 is present. Two carbonyl oxygen atoms of Thr137 and His180 and three side-chain oxygen atoms of Asn101 and Asp146 in a bidentate mode are the ligands, forming a pentagon ring. These ligand residues are conserved except Thr137. In the BSUA structure, one water molecule occupies one side of an apical position of the pentagon and is anchored by the hydrogen bonds with Thr149 and Glu182. The architecture of this calcium binding may be regarded as a pentagonal bipyramid, although another water molecule is not visible in the electron density. His102 adjacent to a ligand residue Asn101 in domain B interacts directly with the substrate and also with a putative catalytic residue Asp176. His180 in domain A interacts with substrate. Thus, Ca-1 serves not only to link the two parts, but also indirectly interacts with substrate. Therefore, Ca-1 could contribute to stabilization of the structure of the active site. Although the effect of calcium on the activity is not prominent in BSUA, calcium protects the enzyme from protease degradation (Takase *et al.*, 1988).

Ca-2 is located at the N-terminal side of $(\beta/\alpha)_8$-barrel and before Aβ4. Ca-3 is an intermolecular calcium ion which is located between the loop before Aα7 and the loop before Aβ3 of the symmetry-related molecule. These calcium binding sites have not been reported in other α-amylases, and seem to be adventitious due to the high concentration of calcium ion used for crystallization. However, Ca-3 binding may be important for the crystal packing formation, because no crystals have been obtained without calcium ion.

Table 5. Coordination of the calcium ions

Site	Atom	Distance (Å)
1	Asp146 OD1	2.7
	Asp146 OD2	2.5
	Asn101 OD1	2.5
	Thr137 O	2.4
	His180 O	2.4
	Wat76	2.4
2	Asp171 OD1	2.6
	Asp171 OD2	2.6
	Gly169 O	2.3
	Wat37	2.5
	Wat49	2.4
	Wat105	2.4
3	Glu276 OE1	2.7
	Glu276 OE2	2.6
	Gly313 O	2.4
	Glu89′ OE2[a]	2.7
	Wat61	2.5
	Wat91	2.4
	Wat93	2.4

[a] Glu89′ is from the adjacent molecule.

Discussion

Our results provide the first atomic description of the interaction between α-amylase and its natural substrate, giving a substantial basis for understanding the first stage of the catalytic reactions.

Identity of the bound sugar

Our procedure for crystallizing the EQ208/G5 complex involved pretreatment of the protein with acarbose and subsequent incubation with G5 in the presence of a small amount of acarbose. A similar procedure was taken by Strokopytov *et al.* (1996) for a fully active mutant of CGTase: crystals were first soaked with acarbose and then maltohexaose. Their structure analysis showed that a new inhibitor, composed of nine saccharide residues, was bound in the active site. Qian *et al.* (1994) reported that crystals of wild-type PPA soaked with acar-

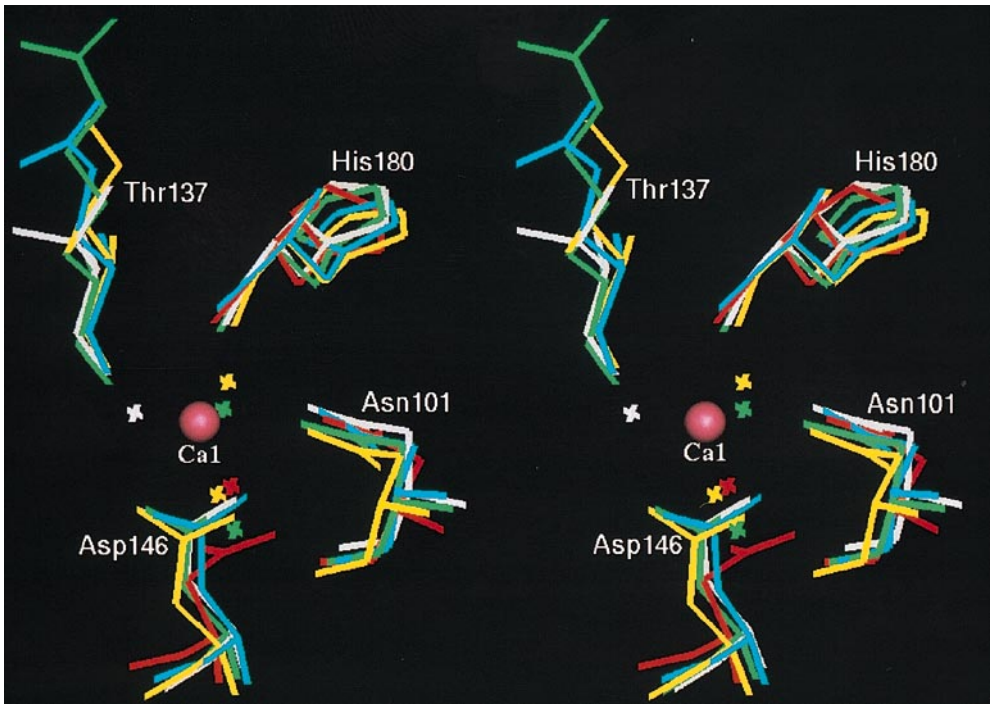

Figure 8. Stereoview of a superposition of the conserved calcium binding site in BSUA (white), PPA (green), TAA (blue) and CGTase (yellow). The equivalent region in BLA (red) is also shown although calcium ion is not present. Cross marks indicate water molecules. Only BSUA residues are labeled.

bose gave a structure with five bound sugar rings, the pseudodisaccharide acarviosine being located at the catalytic center. Brzozowski and Davies (1997) found a hexasaccharide inhibitor bound in the active site of TAA soaked with acarbose. These transformations are thought to occur as a result of transglycosylation activity of α-amylase, and we have previously pointed out such possibility also in wild-type BSUA when incubated with both acarbose and G5 (Takase *et al.*, 1992). Although EQ208 is a catalytic-site mutant, the present sample had a slight residual activity and a possibility exists that the processing of acarbose might have occurred during crystallization.

The present electron density maps at 2.5 Å resolution did not allow us to distinguish between glucose and a pseudosaccharide unit for the bound pentasaccharide molecule, so there remains a problem of whether the bound sugar is G5 or an acarbose-derived inhibitor, which must be solved experimentally in future studies (the possibility of unprocessed acarbose may be excluded because only a molecule with five sugar rings was found in the X-ray structure). However, existing biochemical data suggest that the bound sugar is quite likely to be a G5 molecule, as follows. In the crystallization of EQ208 coincubated with G5 and acarbose, there was no sign of modification or degradation having occurred in either G5 or acarbose when analyzed by thin layer chromatography. The large G5 spot corresponding to the original composition persisted throughout the crystallization period (see Materials and Methods). The wild-type BSUA cannot degrade or trim acarbose to produce transglycosylated derivatives in detectable amounts. When G5 and acarbose were incubated with the wild-type enzyme under conditions similar to the crystallization of EQ208, the G5 spot diminished to a minor spot, which shows that a possible transglycosylation product of acarbose (= acarbose*) does not give a large spot at the G5 position. Thus, it is concluded that G5 was present at high concentration in the crystallization mixture of EQ208 after long periods of incubation. On the other hand, acarbose* should be present, if at all, at extremely low concentration in the crystallization of EQ208 because the trace activity of the EQ208 sample is even lowered 1000-fold by the presence of acarbose. Our previous studies using acarbose* affinity chromatography showed that the EQ208 protein eluted easily from the column by washing with 10 mM G5, while the wild-type enzyme was firmly retained, which shows preferential binding of G5 to EQ208 in the presence of acarbose* and preferential binding of acarbose* to the wild-type enzyme in the presence of G5 (Takase, 1992; Takase *et al.*, 1992). Acarbose has even lower affinities for both EQ208 and the wild-type enzyme than acarbose*. Thus, in the final crystallization mixture of EQ208 where a high concentration of G5, a moderate concentration of acarbose, and a very low concentration of acarbose* are present, it is expected that EQ208 is complexed with G5, which can replace the pre-bound acarbose or acarbose*. The contaminating wild-type(-like) enzyme, which amounts to only 0.005% of EQ208 (Takase

et al., 1992), is expected to be complexed with acarbose or acarbose* so that its activity to degrade G5 is inhibited (see Materials and Methods).

Substrate binding and catalytic implications

The structure of the EQ208/G5 complex has revealed the hydrogen-bonding interactions between individual Glc residues and protein, some of which are not entirely predictable from previous studies (Table 2 and Figure 6). Glc3 is tightly bound near the catalytic-site residues Asp176, Gln208 and Asp269. The amide nitrogen NE2 of Gln208 makes a hydrogen bond with the glucosidic oxygen in the scissile bond between Glc3 and Glc4. This hydrogen-bonding manner may correspond to that of the protonated state of Glu208 in the initial kinetic complex between wild-type enzyme and substrate. The latter hydrogen bonding must be transient and would facilitate the proton transfer event. Thus, Glu208 is likely to act as a general acid. On the other hand, the amide oxygen OE1 of Gln208 makes hydrogen bonds with the main-chain NH of Ala177 and a bound water. The formation of these hydrogen bonds is possible also for Glu208 in wild-type by using OE2. These hydrogen bonds are likely to serve as anchors for making the amide proton (protonated OE1-H in Glu208) point precisely to the glucosidic oxygen in the scissile bond.

The carboxyl group of Asp176 has non-bonded contacts to the anomeric carbon atom C1 (distance 3.0 Å) and to the endocyclic oxygen atom O5 (distance 3.2 Å) of Glc3. Thus, Asp176 could serve as a general base, stabilizing the putative oxocarbonium ion formed after cleavage of the substrate. This rationalizes a complete loss of activity when Asp176 is mutated to a neutral-charged Asn. These assignments of catalytic residues are consistent with the structures of PPA complexed with acarbose (Qian *et al.*, 1994) and CGTase complexed with acarbose (Strokopytov *et al.*, 1995). A conception of the roles of these residues is based on the general acid–base mechanism originally proposed for hen egg-white lysozyme by Phillips and co-workers (Blake *et al.*, 1967a,b).

The carboxyl group of Asp269 participates in hydrogen bonds to the O2 and O3 hydroxyl groups of Glc3, showing a role as substrate binding. Our previous studies showed that the dissociation constant of G5 for DN269 [Asp269 → Asn] is close to the K_m for the wild-type enzyme (Takase, 1992), suggesting a possibility of similar hydrogen bonds using the side-chain amide group of Asn269. Critical roles in catalysis remain uncertain. Asp328 in CGTase (analogous to Asp269 in BSUA) is thought to elevate the pK_a of Glu257 (analogous to Glu208) through a direct hydrogen bond with a proton in between the carboxyl groups of the two residues in uncomplexed state. The catalytic role of Asp269 in BSUA will become clear when the structure of the uncomplexed state of the wild-type enzyme is determined.

Replacement of His180 by a shorter amino acid residue of Asn would disrupt a hydrogen bond with Glc4, since ND2 of the replaced Asn cannot approach more closely than 3.8 Å to O2 of Glc4 even by adjustment of the torsion angles of the side-chain of this Asn residue. The loss of this hydrogen bond must have an influence on the affinity and its precise positioning of the substrate. In mutagenesis and kinetic studies, His180 → Asn mutation gave a 20-fold reduction of k_{cat} with a fivefold increase in K_m for a G5 derivative (Takase *et al.*, 1992). It is thus concluded that His180 makes a hydrogen bond with the substrate and places the substrate in the precise position in the active site.

Arg174, which is strictly conserved in all α-amylases and CGTases, makes a hydrogen bond with O2 of Glc3. Interactions of this residue with carbohydrate have not been reported previously. The corresponding residues in mammalian α-amylases and BLA coordinate to a chloride ion (Qian *et al.*, 1993; Brayer *et al.*, 1995; Machius *et al.*, 1995; Ramasubbu *et al.*, 1996). In BSUA, a chloride ion at this site was not observed although calcium chloride was used in the crystallization.

The dissociation constant of G5 for EQ208 was about 1/100 of those for DN176 and DN269 and the K_m for wild-type, which implied that G5 binds to EQ208 more tightly than to wild-type, DN176 and DN269 (Takase, 1992). This is partly explicable by the formation of a stable hydrogen bond between the glucosidic oxygen O4(4) and NE2 of Gln208. On the other hand, acarbose binds to wild-type more tightly than to EQ208 (Takase, 1992; Takase *et al.*, 1992). In this case, the carboxyl oxygen of Glu208 could serve as a hydrogen bond acceptor from the glucosidic NH of the acarviosine group, but the NE2 of Gln208 could not.

In addition to the hydrogen bonding interactions, there are many hydrophobic residues involved in G5 binding (Table 3). These residues serve to form the framework of the substrate binding cleft as well as to interact directly with the sugar residues. Three leucine residues, Leu141, Leu142 and Leu144, form the inner curvature of the binding cleft and fit snugly into the dent of the G5 molecule. Aromatic residues, Trp and Tyr, build the walls of the cleft and most of them appear to have stacking interactions with sugar residues. The phenyl ring of Tyr62 stacks with the glucose ring of Glc3. This residue is conserved among the α-amylase family and is close to Asp176, one of the catalytic-site residues. So, the stacking interaction must be important in both substrate binding and catalysis. Indeed, Matsui *et al.* (1994) found in *Saccharomycopsis* α-amylase that substitution of Tyr83 (corresponding to Tyr62 in BSUA) with Leu or Asn caused substantial loss of activity. Previously, we observed difference absorption spectra of catalytic-site mutants with

Table 6. Native and heavy-atom derivative data statistics

Data set	Resolution (Å)	Total reflections	Unique reflections	Completeness (%)	*R*-merge (%)	*R*-difference (%)	Phasing power		Cullis *R*-factor		Site
							Centric	Acentric	Centric	Acentric	
Native	2.5	56,354	18,097	80	6.7						
K_2PtCl_4 no.1	2.5	59,951	18,483	82	8.4	9.2	1.20	1.42	0.64	0.74	7
K_2PtCl_4 no.2	3.0	48,338	9,937	74	8.0	7.8	1.30	1.20	0.64	0.82	6
$HgCl_2$	2.5	92,920	20,247	88	9.0	10.3	1.06	1.00	0.70	0.84	3

R-merge $= \Sigma\Sigma|I_i - \langle I\rangle| / \Sigma\langle I\rangle$.
R-difference $= \Sigma||F_{ph}| - |F_p|| / \Sigma|F_p|$.
Phasing power = r.m.s. F_h/(r.m.s. lack of closure); F_h, calculated heavy-atom structure factor.
Cullis R-factor $= \Sigma||F_{ph} - F_p| - |F_h|| / \Sigma|F_{ph} - F_p|$.

G5 which showed perturbations of Trp and Tyr upon G5 binding (Takase, 1992). The structure revealed in the present study pinpoints those Trp and Tyr residues. The spectra of the three mutants differed from each other in their shape and intensity, which is ascribed to the mutation of each catalytic-site residue, Asp176, Glu208 and Asp269, to its amide form. As Trp58 and Tyr62 are close to Asp269 and Asp176, respectively, their environments are most likely to be affected by the respective mutation. Thus, it may be assumed that Trp58 and Tyr62 contribute to the difference spectra significantly. Trp58 is not conserved among the α-amylase family and is found in only a few α-amylases including PPA.

Materials and Methods

Enzyme preparation and crystallization

The EQ208 mutant protein was produced in the *B. subtilis* expression system and purified from the culture supernatant as described previously (Takase *et al.*, 1992). Two forms of protein, N42 and N40, can be produced through different NH_2-terminal processings (Takase *et al.*, 1988), where N42 is the final mature form and N40 has two extra NH_2-terminal residues (numbered −2 and −1). The N40 form was used in the present study. The purified EQ208 sample exhibited a trace amount of activity (about 0.005% of the wild-type enzyme) which was considered to originate from contamination by the wild-type enzyme (Takase *et al.*, 1992). To suppress the residual activity during crystallization, it was first treated with acarbose, a pseudotetrasaccharide α-amylase inhibitor, before mixing with G5 as described below. Under these conditions, it is expected that acarbose binds to the wild-type enzyme selectively, while G5 binds to EQ208 (Takase, 1992; Takase *et al.*, 1992; also see Discussion).

Crystallization trials of the EQ208/G5 complex were undertaken according to the hanging-drop vapor diffusion method (Mizuno *et al.*, 1993). 16.4 mg/ml EQ208 in 10 mM Tris-HCl (pH 7.5) buffer containing 3.5 mM $CaCl_2$ was mixed with the 1/20 volume of 2% acarbose and incubated for 30 minutes at room temperature. Subsequently, G5 was added to the solution so that the final G5 concentration became 0.09 to 1.23% and incubation continued for 20 minutes. A droplet of 4 μl of this solution mixed with an equal volume of reservoir solution of 10% polyethylene glycol 3350 in the same buffer was set to equilibrate with the reservoir at 20°C. Crystals grew as rods within 2 weeks under several conditions. The largest crystals of dimensions about 0.3 mm × 0.4 mm × 1.0 mm were obtained when 1.3% EQ208 and 0.32% G5 were employed. The sugar composition of the crystallized solutions was analyzed by thin layer chromatography. Only a large G5 spot and a faint acarbose spot as expected for the original composition were observed, with no significant changes from the first day through 90 days incubation, which ensured that G5 was not degraded during crystallization. These crystals belong to the orthorhombic space group $P2_12_12_1$ with cell constants $a = 72.6$ Å, $b = 74.1$ Å and $c = 117.0$ Å, and contain one molecule in the asymmetric unit (Table 1).

G5 was purchased from Seikagaku Kogyo Co. Ltd. Acarbose was generously supplied as a gift by Bayer.

X-ray data collection and processing

Diffraction experiments were carried out at the Photon Factory in Tsukuba. The data were collected on an imaging plate mounted on a Weissenberg camera designed for macromolecules (Sakabe, 1991) on beam line BL6A. The wavelength used was 1.00 Å, and the collimator was 0.1 mm. These data were processed using the program DENZO and scaled using the program SCALEPACK (Otwinowski, 1993). The collected native intensity data set contained a total of 56,354 observations, which reduced to 18,097 unique reflections with 80% completeness and a merging R-factor of 6.7% on intensities (Table 6). Heavy-atom derivative data were also collected in the same way and scaled to the native data.

Heavy-atom derivatives and multiple isomorphous replacement

Heavy-atom crystals were prepared by conventional soaking methods. The heavy-atom compound was dissolved in mother liquor at a final concentration of 1 to 3 mM. Soaked crystals were left at room temperature for 3 days. The interpretation of potential heavy-atom derivatives was initially done using self-vector verification of three-dimensional difference Patterson functions with PHASES program package (Furey & Swaminathan, 1990). One Pt position of the K_2PtCl_4 derivative was clearly obtained from the Patterson maps. The Hg positions of the $HgCl_2$ derivative were then obtained from

difference Fourier maps made with single isomorphous replacement phases from the platinum derivative. A total of seven Pt and three Hg positions were obtained. These heavy-atom parameters were refined and phases were computed with the program MLPHARE (Otwinowski, 1991) in a CCP4 program package (Collaborative Computational Project, 1994) using reflections from 50 to 2.5 Å resolution. Data collection and heavy-atom refinement statistics are shown in Table 6. The obtained phases were used to calculate an electron density map. The multiple isomorphous replacement (MIR) map was improved by solvent flattening and density modifications using the program DM (Cowtan, 1994) in a CCP4 program package.

Model building and structure refinement

Building of the C^{α} atom models in this map was initially conducted referring to the model of TAA starting at the $(\beta/\alpha)_8$-barrel in domain A, and finally the C^{α} positions of the entire polypeptide chain were traced unambiguously using the program X-fit in QUANTA/X-RAY package (Version 4.0, Molecular Simulations, Inc.), except terminal residues −2, −1 and 426 to 436 as they could not be assigned because of no density. The C^{α} atom model was then converted to the appropriate sequence model by energy restrained crystallographic refinement. The obtained model was verified by MIR maps, and manual model rebuilding particularly in side-chains was required. Residues 1 to 425 were rebuilt and used as a starting model for refinement. Positional and simulated annealing refinement were performed on the model with the program XPLOR (Brünger *et al.*, 1987). The stereochemical parameter set of Engh and Huber (1991) was used for protein refinement cycles. The difference $F_{obs} - F_{calc}$ and $2F_{obs} - F_{calc}$ maps were calculated as reference for model adjustment. During the course of the refinement, $F_{obs} - F_{calc}$ maps were calculated to identify the presence of the bound sugar ligand, and clear connected density corresponding to G5 was found in the active site of the EQ208. Similarly, calcium ions were identified. The G5 molecule and two calcium ions were added to the model over several refinement cycles. One of new peaks in the subsequent $F_{obs} - F_{calc}$ maps was assigned as another calcium ion and the remaining peaks as water molecules if they exceeded 3 σ in the maps at appropriate distances from protein atoms. Subsequent refinement was carried out using native data set up to a resolution of 2.5 Å. The free *R*-factor, which was calculated by setting aside 10% of the reflection data, was used as a guide throughout refinement (Table 1). Stereochemistry of the model was analyzed with the program PROCHECK (Laskowski *et al.*, 1992). The coordinates have been deposited in the Protein Data Bank under file name 1BAG.

Acknowledgments

This work was done with the approval of the Photon Factory Advisory Committee, the National Laboratory for High Energy Physics, Tsukuba (proposal 94G-037 and 96G-044). We thank Professor Sakabe, Drs Nakagawa, Watanabe and Suzuki for help in data collection at the Photon Factory, and Professors Tsukihara and Morimoto for valuable discussions. H.M. is a member of the TARA (Tsukuba Advanced Research Alliance) Project of the University of Tsukuba, Japan. This work was supported by Special Coordination Funds for Promoting Science and Technology of STA (H.M.)

References

Banner, D. W., Bloomer, A. C., Petsko, G. A., Phillips, D. C., Pogson, C. I., Wilson, I. A., Corran, P. H., Furth, A. J., Milman, D. J., Offord, R. E., Priddle, J. D. & Waley, S. G. (1975). Structure of chicken muscle triose phosphate isomerase determined crystallographically at 2. 5 Å resolution using amino acid sequence data. *Nature,* **255**, 609–614.

Blake, C. C. F., Mair, G. A., North, A. C. T., Phillips, D. C. & Sarma, V. R. (1967a). On the conformation of the hen egg-white lysozyme molecule. *Proc. R. Soc. ser. B*, **167**, 365–377.

Blake, C. C. F., Johnson, L. N., Mair, G. A., North, A. C. T., Phillips, D. C. & Sarma, V. R. (1967b). Crystallographic studies of the activity of hen egg-white lysozyme. *Proc. R. Soc. ser. B,* **167**, 378–388.

Boel, E., Brady, L., Brzozowski, A. M., Derewanda, Z., Dodson, G. G., Jensen, V. J., Petersen, S. B., Swift, H., Thim, L. & Woldike, H. F. (1990). Calcium binding in α-amylases: an X-ray diffraction study at 2. 1–Å resolution of two enzymes from *Aspergillus*. *Biochemistry,* **29**, 6244–6249.

Brady, R. L., Brzozowski, A. M., Derewanda, Z. S., Dodson, E. J. & Dodson, G. G. (1991). Solution of the structure of *Aspergillus niger* acid α-amylase by combined molecular replacement and multiple isomorphous replacement methods. *Acta Crystallog. sect. B,* **47**, 527–535.

Brayer, G. D., Luo, Y. & Withers, S. G. (1995). The structure of human pancreatic α-amylase at 1. 8 Å resolution and comparisons with related enzymes. *Protein Sci.* **4**, 1730–1742.

Brzozowski, A. M. & Davies, G. J. (1997). Structure of the *Aspergillus oryzae* α-amylase complexed with the inhibitor acarbose at 2. 0 Å resolution. *Biochemistry,* **36**, 10837–10845.

Brünger, A. T., Kuriyan, J. & Karplus, M. (1987). Crystallographic *R* factor refinement by molecular dynamics. *Science,* **235**, 458–460.

Brünger, A. T. (1992). Free *R* value: a novel statistical quantity for assessing the accuracy of crystal structures. *Nature,* **355**, 472–475.

Collaborative Computational Project N. (1994). The CCP4 Suite: Programs for protein crystallography. *Acta Crystallog. sect. D,* **50**, 760–763.

Cowtan, K. (1994). CCP4 density modification package. In *Joint CCP4 and ESF-EACBM Newsletter on Protein Crystallography* 31, pp. 34–38.

Dowd, M. K., Zeng, J., French, A. D. & Reilly, P. J. (1992). Conformational analysis of the anomeric forms of kojibiose, nigerose, and maltose using MM3. *Carbohyd. Res.* **230**, 223–244.

Engh, R. A. & Huber, R. (1991). Accurate bond and angle parameters for X-ray protein structure refinement. *Acta Crystallog. sect. A,* **47**, 392–400.

Furey, W. & Swaminathan, S. (1990). PHASES, a program package for the processing and analysis of diffraction data from macromolecules. *Am. Crystallog. Assoc. Meet. Abs. ser. 2,* **18**, 73.

Hiromi, K., Ohnishi, M. & Tanaka, A. (1983). Subsite structure and ligand binding mechanism of glucoamylase. *Mol. Cell. Biochem.* **51**, 79–85.

Holm, L., Koivula, A. K., Lehtovaara, P. M., Hemminki, A. & Knowles, J. K. C. (1990). Random mutagenesis used to probe the structure and function of *Bacillus stearothermophilus* alpha-amylase. *Protein Eng.* **3**, 181–191.

Hwang, K. Y., Song, H. K., Chang, C., Lee, J., Lee, S. Y., Kim, K. K., Choe, S., Sweet, R. M. & Suh, S. W. (1997). Crystal structure of thermostable α-amylase from *Bacillus licheniformis* refined at 1. 7 Å resolution. *Mol. Cells,* **7**, 251–258.

Kadziola, A., Abe, J., Svensson, B. & Haser, R. (1994). Crystal and molecular structure of barley α-amylase. *J. Mol. Biol.* **239**, 104–121.

Klein, C., Hollender, J., Bender, H. & Schulz, G. E. (1992). Catalytic center of cyclodextrin glycosyltransferase derived from X-ray structure analysis combined with site-directed mutagenesis. *Biochemistry,* **31**, 8740–8746.

Knegtel, R. M. A., Strokopytov, B., Penninga, D., Faber, O. G., Rozeboom, H. J., Kalk, K. H., Dijkhuizen, L. & Dijkstra, B. W. (1995). Crystallographic studies of the interaction of cyclodextrin glycosyltransferase from *Bacillus circulans* strain 251 with natural substrates and products. *J. Biol. Chem.* **270**, 29256–29264.

Kraulis, P. J. (1991). MOLSCRIPT: a program to produce both detailed and schematic plots of protein structures. *J. Appl. Crystallog.* **24**, 946–950.

Larson, S. B., Greenwood, A., Cascio, D., Day, J. & McPherson, A. (1994). Refined molecular structure of pig pancreatic α-amylase at 2. 1 Å resolution. *J. Mol. Biol.* **235**, 1560–1584.

Laskowski, R. A., MacArthur, M. W., Moss, D. S. & Thornton, J. M. (1992). *PROCHECK v.2: Programs to check the Stereochemistrial Quality of Protein Structures,* Oxford Molecular Ltd, Oxford, England.

Luzzati, P. V. (1952). Traitement statistique des erreurs dans la determination des structures cristallines. *Acta Crystallog.* **5**, 802–810.

Machius, M., Wiegand, G. & Huber, R. (1995). Crystal structure of calcium-depleted *Bacillus licheniformis* α-amylase at 2.2 Å resolution. *J. Mol. Biol.* **246**, 545–559.

Machius, M., Lazsló Vértesy, Huber, R. & Wiegand, G. (1996). Carbohydrate and protein-based inhibitors of porcine pancreatic α-amylase: structure analysis and comparison of their binding characteristics. *J. Mol. Biol.* **260**, 409–421.

Matsui, I., Yoneda, S., Ishikawa, K., Miyairi, S., Fukui, S., Umeyama, H. & Honda, K. (1994). Roles of the aromatic residues conserved in the active center of *Saccharomycopsis* α-amylase for transglycosylation and hydrolysis activity. *Biochemistry,* **33**, 451–458.

Matsuura, Y., Kusunoki, M., Harada, W. & Kakudo, M. (1984). Structure and possible catalytic residues of Taka-amylase A. *J. Biochem.* **95**, 697–702.

Mizuno, H., Morimoto, Y., Tsukihara, T., Matsumoto, T. & Takase, K. (1993). Crystallization and preliminary X-ray studies of wild type and catalytic-site mutant α-amylase from *Bacillus subtilis*. *J. Mol. Biol.* **234**, 1282–1283.

Nicholls, A. (1992). *GRASP: Graphical Representation and Analysis of Surface Properties,* Columbia University, New York.

Otwinowski, Z. (1991). Isomorphous replacement and anomalous scattering. *Proceedings of the CCP4 Study Weekend* (Wolf, W., Evans, P. R. & Leslie, A. G. W., eds), pp. 80–88, SERC Daresbury Laboratory, Warrington, UK.

Otwinowski, Z. (1993). Data Collection and Processing. *Proceedings of the CCP4 Study Weekend.* (Sawyer, L., Isaacs, N. & Bailey, S., eds), pp. 56–62, SERC Daresbury Laboratory, Warrington, UK.

Qian, M., Haser, R. & Payan, F. (1993). Structure and molecular refinement of pig pancreatic α-amylase at 2.1 Å resolution. *J. Mol. Biol.* **231**, 785–799.

Qian, M., Haser, R., Buisson, G., Dúee, E. & Payan, F. (1994). The active center of a mammalian α-amylase. Structure of the complex of a pancreatic α-amylase with a carbohydrate inhibitor refined to 2.2–Å resolution. *Biochemistry,* **33**, 6284–6294.

Qian, M., Haser, R. & Payan, F. (1995). Carbohydrate binding sites in a pancreatic α-amylase-substrate complex, derived from X-ray structure analysis at 2.1 Å resolution. *Protein Sci.* **4**, 747–755.

Ramachandran, G. N. & Sasisekharan, V. (1968). Conformation of polypeptides and proteins. *Advan. Protein Chem.* **23**, 283–437.

Ramasubbu, N., Paloth, V., Luo, Y., Brayer, G. D. & Levine, M. J. (1996). Structure of human salivary α-amylase at 1. 6 Å resolution: Implications for its role in the oral cavity. *Acta Crystallog. sect. D,* **52**, 435–446.

Robyt, J. F. & French, D. (1970). The action pattern of porcine pancreatic α-amylase in relationship to the substrate binding site of the enzyme. *J. Biol. Chem.* **245**, 3917–3927.

Sakabe, N. (1991). X-ray diffraction data collection system for modern protein crystallography with a Weissenberg camera and an imaging plate using synchrotron radiation. *Nuclear Instr. Methods Physics Res.* **A303**, 448–463.

Strokopytov, B., Penninga, D., Rozeboom, H. J., Kalk, K. H., Dijkhuizen, L. & Dijkstra, B. W. (1995). X-ray structure of cyclodextrin glycosyltransferase complexed with acarbose. Implications for the catalytic mechanism of glycosidases. *Biochemistry,* **34**, 2234–2240.

Strokopytov, B., Knegtel, R. M. A., Penninga, D., Rozeboom, H. J., Kalk, K. H., Dijkhuizen, L. & Dijkstra, B. W. (1996). Structure of cyclodextrin glycosyltransferase complexed with a maltononaose inhibitor at 2. 6 Å resolution. Implications for product specificity. *Biochemistry,* **35**, 4241–4249.

Swift, H. J., Brady, L., Derewanda, Z. S., Dodson, E. J., Dodson, G. G., Turkenburg, J. P. & Wilkinson, A. J. (1991). Structure and molecular model refinement of *Aspergillus oryzae*(TAKA) α-amylase: an application of the simulated-annealing method. *Acta Crystallog. sect. D,* **47**, 535–544.

Søgaard, M., Kadziola, A., Haser, R. & Svensson, B. (1993). Site-directed mutagenesis of histidine 93, aspartic acid 180, glutamic acid 205, histidine 290, and aspartic acid 291 at the active site and tryptophan 279 at the raw starch binding site in barley α-amylase 1. *J. Biol. Chem.* **268**, 22480–22484.

Takase, K., Mizuno, H. & Yamane, K. (1988). NH_2-terminal processing of *Bacillus subtilis* α-amylase. *J. Biol. Chem.* **263**, 11548–11553.

Takase, K. (1992). Interaction of catalytic-site mutants of *Bacillus subtilis* α-amylase with substrates and acarbose. *Biochim. Biophys. Acta,* **1122**, 278–282.

Takase, K., Matsumoto, T., Mizuno, H. & Yamane, K. (1992). Site-directed mutagenesis of active site residues in *Bacillus subtilis* α-amylase. *Biochim. Biophys. Acta,* **1120**, 281–288.

Takusagawa, F. & Jacobson, R. A. (1978). The crystal and molecular structure of α-maltose. *Acta Crystallog. sect. B*, **34**, 213–218.

Vihinen, M., Ollikka, P., Niskanen, J., Meyer, P., Suominen, I., Karp, M., Holm, L., Knowles, J. & Mäntsälä, P. (1990). Site-directed mutagenesis of a thermostable α-amylase from *Bacillus stearothermophilus*: putative role of three conserved residues. *J. Biochem.* **107**, 267–272.

Yoshioka, Y., Hasegawa, K., Matsuura, Y., Katsube, Y. & Kubota, M. (1997). Crystal structure of a mutant maltotetraose-forming exo-amylase cocrystallized with maltopentaose. *J. Mol. Biol.* **271**, 619–628.

Edited by R. Huber

(Received 26 August 1997; received in revised form 28 December 1997; accepted 1 January 1998)